Interpretation of the response of cryogenic rocket flames to forced acoustics using large eddy simulation

By Justin HARDI[1], Youhi MORII[2], Scott BEINKE[1,3], Taro SHIMIZU[2], Hideto KAWASHIMA[4], and Michael OSCHWALD[1,5]

[1]*Institute of Space Propulsion, DLR, Lampoldshausen, Germany*
[2]*JEDI Center, JAXA, Kanagawa, Japan*
[3]*School of Mechanical Engineering, The University of Adelaide, Adelaide, Australia*
[4]*Space Technology Directorate I, JAXA, Tsukuba, Japan*
[5]*Institute of Jet Propulsion and Turbomachinery, RWTH, Aachen, Germany*

Experimental measurement of flame response to acoustics under conditions relevant to industrial engines is challenging and so the scope of such measurements is often limited. High fidelity CFD can be used to model the interaction of acoustic waves with cryogenic flames, and modelling an experimental test case can not only serve as a code validation exercise but also be useful in better characterising the experimental results. This work explores this potential by extending the interpretation of high-speed imaging of representative rocket flames based on comparison with a large eddy simulation of the experiment.

Nomenclature

D	:	inner diameter of oxygen injector, mm
J	:	momentum flux ratio $\rho_H u_H^2 / \rho_O u_O^2$
M	:	per-element mass flow rate, g/s
μ	:	dynamic viscosity, Pa.s
p'	:	dynamic (acoustic) pressure, bar
P	:	mean pressure, bar
ρ	:	density, kg/m^3
Re_D	:	oxygen injection Reynolds number $\rho_O u_O D / \mu_O$
ROF	:	ratio of oxidiser-to-fuel mass flow
T	:	temperature, K
u	:	injection velocity, m/s
u'	:	acoustic velocity amplitude, m/s
VR	:	ratio of fuel-to-oxidiser injection velocity

Subscripts

cc	:	combustion chamber
O	:	oxygen
H	:	hydrogen

1. Introduction

High frequency (HF) combustion instability can occur in liquid propellant rocket engines when acoustic oscillations and unsteady energy release from combustion become coupled. While generally considered to have good stability characteristics, engines using the propellant combination liquid oxygen/hydrogen (LOx/H$_2$) with shear coaxial injectors are not immune to the problem.[1]–[3]

Understanding of high frequency combustion instabilities in liquid propellant rocket engines would benefit from detailed measurements of flame response to high amplitude acoustics. Experiments striving to observe flames under representative operating conditions often use siren excitation of the combustion chamber to force transverse-mode acoustic resonance.[4]–[8] Shadowgraph imaging from such experiments has revealed significant response of the LOx jets, or 'cores', to transverse instability. The intact core shortens in length due to accelerated breakup and mixing driven by the transverse acoustic gas oscillations.[4],[5],[9] Simultaneous filtered flame radiation imaging shows corresponding change in the extent, emission intensity, and dynamics of the flame.[10]

While such observations of the flow field or flame radiation in combustion chambers are possible, the extreme conditions characteristic of rocket combustion often limit the scope of the measurements. Direct, local property measurements are usually impossible. The spatial extent of optical access windows may be limited. Furthermore, two-dimensional observations from a single point of view are insufficient to describe the three-dimensional character of the response.

Numerical modelling using large eddy simulation (LES) offers a way to study flame-acoustic interaction in more detail than is accessible in such experiments. To this end, DLR and JAXA collaborate by exchanging experimental test cases and results from numerical modelling. The current work concerns the test case from a DLR experimental combustor designated 'BKH'.[11] Work on this test case began in the frame of the 3rd Modelling Workshop of the Rocket Engine Stability iniTiative (REST), a cooperation of French and German industrial and institutional partners.[12]

The experimental data originate from a test campaign operated with BKH at the European Research and Technology Test Facility P8 for cryogenic rocket engines at DLR Lampoldshausen. The combustor, illustrated in Fig. 1, is specially designed for visualising the response of rocket
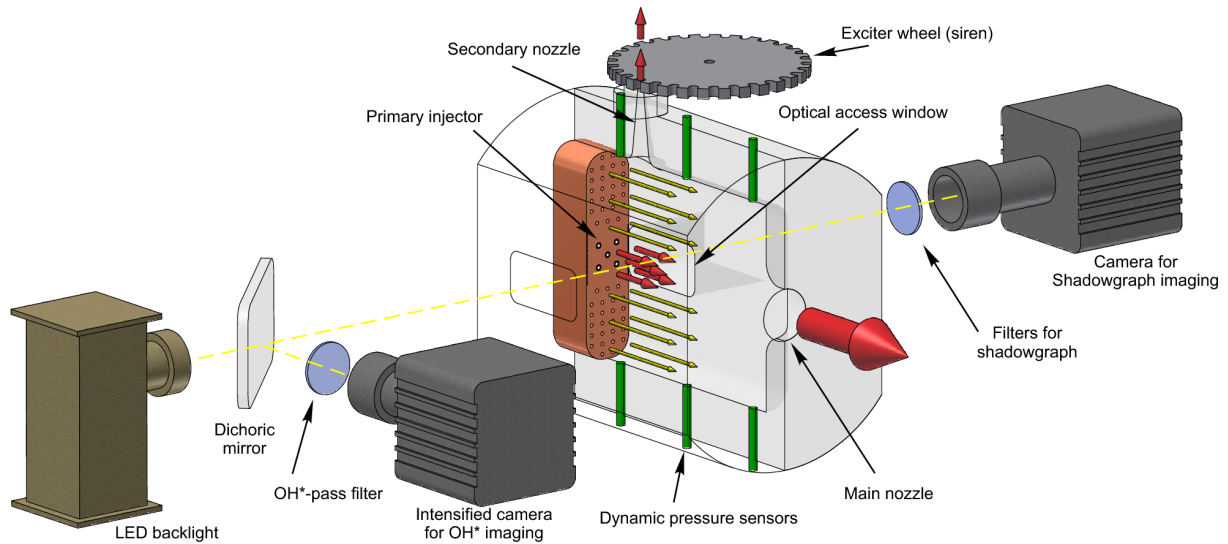
Fig. 1. Conceptual illustration of the experimental combustor, BKH, and optical setup.

flames under simulated conditions of high-frequency combustion instability. The combustor has a rectangular cross-section in order to provide well defined acoustic resonance frequencies and mode structures. It has multiple shear coaxial injection elements with injection parameters representative of upper-stage, LOx/H_2 engines. The injector dimensions are illustrated in Fig. 2. Acoustic forcing with the siren achieves transverse mode acoustic pressure amplitudes up to 9% of mean chamber pressure (18% peak-to-peak), which is representative of dangerous, naturally occurring instabilities. Optical access windows allow high-speed imaging with shadowgraph and filtered flame radiation techniques.

In this work, the spatial and temporal character of the observed flame response phenomena will be compared with results from LES modelling of BKH, performed by JAXA/JEDI. It is not the intention to perform a validation exercise; that work is concurrently nearing completion. Rather, we wish to explore what can be learned about the experiment from the model. Flame response phenomena can be studied in detail in the LES since all locations and variables in the solution field are accessible. Through the comparison of the numerical prediction with the experimental data presented here, it is intended to more fully explain the observations in the experimental data, thereby providing a stronger basis for their use in model validation or in low order models.

Here, the scope is limited to an examination of the shadowgraph images. First, the steady-state flow field is considered with time-averaged imaging and numerical results. Then, the atomisation of the dense oxygen jets during transverse-mode excitation is explained through the comparison of time-resolved numerical results and phase-averaged shadowgraph imaging.

2. Experimental test case

Testing was conducted using the BKH experimental rocket combustor at the European Research and Technology Test
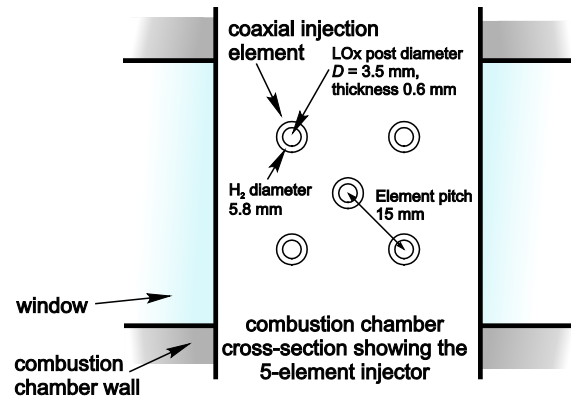

Fig. 2. BKH injector dimensions.

Facility P8 for cryogenic rocket engines at DLR Lampoldshausen. BKH has a rectangular cross-section in order to fix the acoustic resonance frequencies and structures, and a secondary nozzle in the upper wall. The exhaust flow through the secondary nozzle is modulated with a toothed siren, or 'exciter', wheel to excite acoustic resonances inside the combustion chamber. Fig. 1 illustrates the main features of BKH. Optical access is provided to the near-injector region. Piezoelectric type dynamic pressure sensors are flush mounted along the upper and lower chamber walls. For further details on all aspects of the BKH system, the reader is directed to Ref. 11).

Injection of LOx/H_2 occurs through five shear coaxial injection elements with dimensions typical of those found in industrial upper stage engines. Element outlet dimensions are indicated in Fig. 2. The elements are arranged in a 'matrix' pattern, with one central element surrounded by the remaining four, evenly spaced. This arrangement of multiple elements was selected in order to create an environment for the central jet which resembles that of an element in an industrial engine, surrounded on all sides by other elements. The interaction of neighbouring flames is representative of the tightly packed arrangement found in industrial engines. Additional H_2 is injected around the cluster of primary elements for cooling
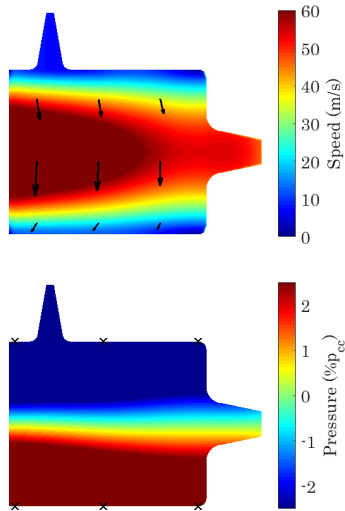
Fig. 3. Acoustic velocity distribution (above) and pressure one-quarter of a cycle later (below) reconstructed from dynamic pressure measurements during peak-amplitude excitation of the first transverse (1T) mode.

Table 1. Experimental conditions.

Mean combustion chamber pressure	P_{CC}	60 bar
Primary injector mixture ratio	ROF	6
Per-element total mass flow rate	M	130 g/s
Oxygen injection temperature	T_O	125 K
Oxygen injection velocity	u_O	12 m/s
Hydrogen injection temperature	T_H	290 K
Hydrogen injection velocity	u_F	420 m/s
Hydrogen/oxygen injection velocity ratio	VR	35
Hydrogen/oxygen momentum flux ratio	J	6
Oxygen injection Reynolds number	Re_O	4×10^5

and flow conditioning purposes.

In this work, imaging results are examined from one operating condition with a combustion chamber pressure (P_{cc}) of 60 bar, a mixture ratio (ROF) of 6, and using hydrogen at ambient temperature. Injection parameters for the test are summarised in Table 1.

Two acoustic cases are examined in this work, one is an unexcited case, where the siren was not in operation, and the other is an excited transverse-mode case. The first transverse (1T) resonance mode of the combustion chamber volume is excited when its frequency is matched by that of the siren wheel teeth passing over the secondary nozzle, at approximately 4200 Hz. In the test data examined here, the amplitude of dynamic pressure (p') in the chamber reached 8.1 bar peak to peak during excitation of the 1T mode.

The acoustic field structure for the 1T mode can be reconstructed from p' measurements taken along the upper and lower chamber walls.[13] The velocity and pressure distributions for peak 1T amplitude, reconstructed through interpolating between p' sensor locations, are shown in Fig. 3. The 1T mode has a pressure nodal line aligned approximately with the main (horizontal) axis of the chamber. This means that exciting this mode subjects the spray flames to high amplitudes of oscillating acoustic gas motion, transverse to the
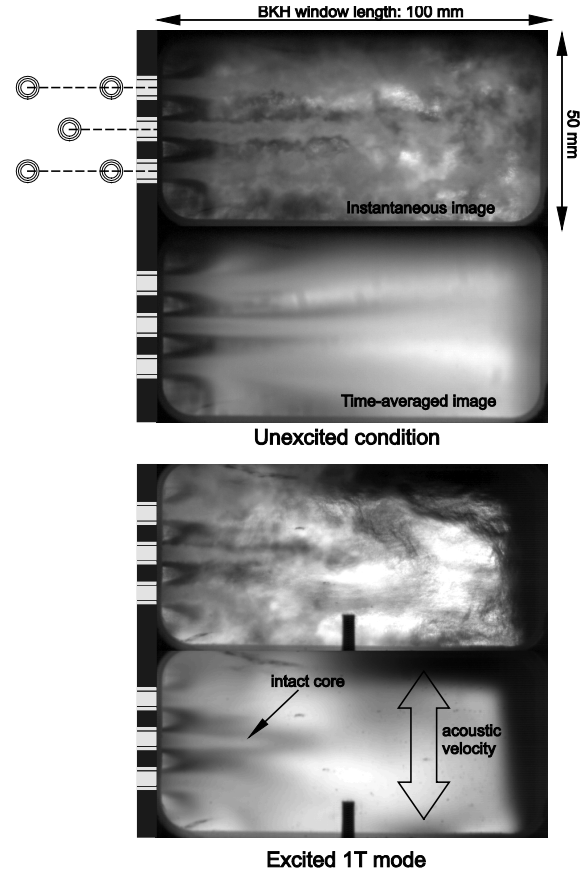

Fig. 4. Instantaneous and time-averaged shadowgraph images from the unexcited case (above) and the excited 1T-mode case (below).

direction of injection.

Observation windows in the walls of BKH provide optical access to the near injector region. Shadowgraph and filtered flame radiation imaging techniques are applied using the setup illustrated schematically in Fig. 1. Instantaneous and time-averaged shadowgraph images from each of these cases are shown in Fig. 4. With injection from the left, the central and two nearest LOx cores are visible. Their boundaries are well defined as light grey on darker immediate surroundings.

The area of optical access measures 50 mm high and 100 mm long, with one side aligned with the injection plane and a height sufficient to view the entire 5-element injector. The dimensions of the window are limited by available film cooling and the axial extent of its effectiveness. As can be seen in Fig. 4, the dense LOx cores penetrate far into the combustion chamber, and the flame spreads transversally (vertically) shortly downstream of the injection plane. This means the transverse and axial extent of the flames is not encompassed by the viewing area of the windows.

3. Numerical model

JAXA employed the unstructured solver FaSTAR[14] to model the BKH test case. The governing equations are three-dimensional filtered compressible Navier-Stokes equations, which include the conservation equations of mass, momentum, energy and mixture fraction. The Large Eddy

Simulation (LES) approach is used with the Wall-Adapting Local Eddy-viscosity (WALE) model.[15] The advection fluxes are evaluated by the SLAU2 scheme,[16] and the viscous and diffusion terms are handled by the central differential formulae with tighter-coupling correction. The time integration is carried out by LU-SGS implicit method with three internal iterations. Single phase fluid is assumed in the simulations. The dense fluid properties are implemented in the original code, in terms of the equation of state (EOS) and the transport coefficients. The Soave-Redlich-Kwon (SRK) EOS is employed. The viscosity and thermal conductivity are modified by the method of Chung.[17] The critical constants are taken from Refs. 18,19).

In this study, we adopt the laminar flamelet concept and alter the chemical reaction calculations by look-up table constructed by detailed one-dimensional counter-flow H_2/O_2 diffusion flame simulations. The 8 species (H_2, O_2, OH, H_2O, H, O, H_2O_2, HO_2) and 21 elementary reaction model,
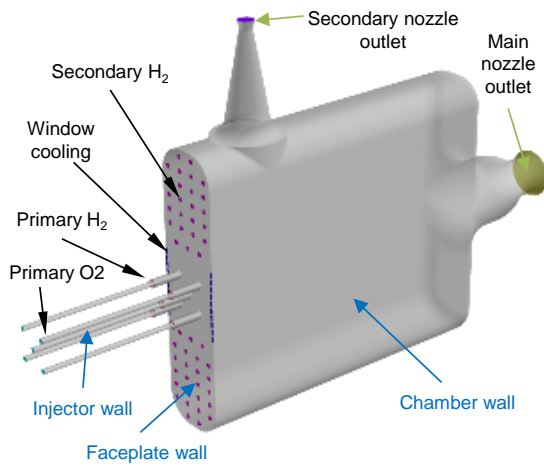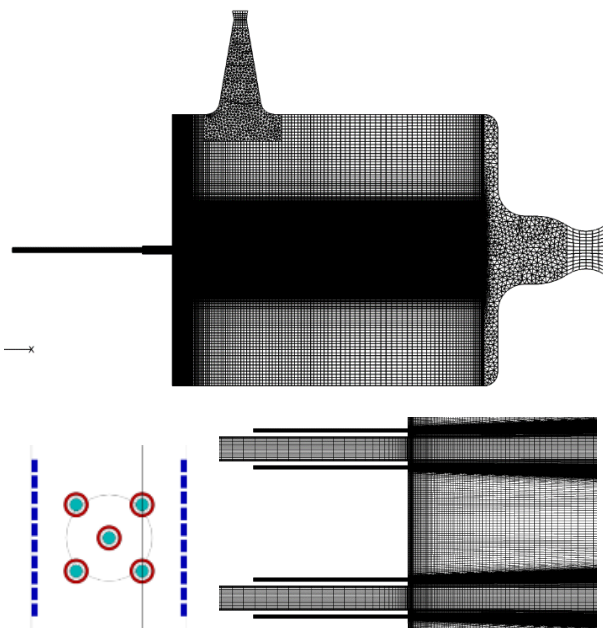
proposed by Li et al.[20] is employed for the H_2/O_2 reaction system at high pressure conditions. The chemistry table used in this study provides the mass fractions of components with the inputs of mixture fraction, scalar dissipation rate and fluctuation of mixture fraction. The mixture fraction is defined by the method of Bilger[21] and the stoichiometric mixture fraction is 0.111.

The computational domain is shown in Fig. 5. The primary injection elements begin after pressure drop (orifice) features near the manifold side. Secondary H_2 and window cooling injectors are simply inlet surfaces on the faceplate. All walls are assumed to be adiabatic. The walls of the injectors and the faceplate are non-slip, and the chamber walls are slip. The primary and secondary nozzle outlets use a zero-order extrapolation condition. For the excited case, the boundary condition at the secondary nozzle outlet is switched between closed and open (with a pressure outlet condition of 1 bar) to simulate the action of the siren teeth.

The domain was meshed with 9.3 M cells. Refinement near the injection plane ensures proper resolution of the shear layer of the primary flames. The minimum grid size was 66 μm. The mesh is illustrated in Fig. 6. This mesh was found to yield results which agree well with the experiment in terms of mean P_{cc}, unexcited chamber acoustics, and flame topology.

4. Results and discussion

4.1. Unexcited case

First, the numerical results from the LES model for the unexcited case are explored for additional information they can provide on the combustion chamber conditions in the experiment. The extent of the dense oxygen jets is visualised in Fig. 7 in terms of O_2 mass fraction distribution. Immediately evident is the extent of transverse (vertical) spreading of the atomising outer jets into the space above and below the injector cluster. The outer jets even recirculate back to the faceplate. This recirculation can also be illustrated effectively by streamlines from the injectors, as in Fig. 8. It explains the 'peeling off' and recirculation of the outer flames at 'shoulders' approximately 15 mm downstream of injection, as indicated by traced lines in the upper half of Fig. 9.

Fig. 5.   Computational domain.

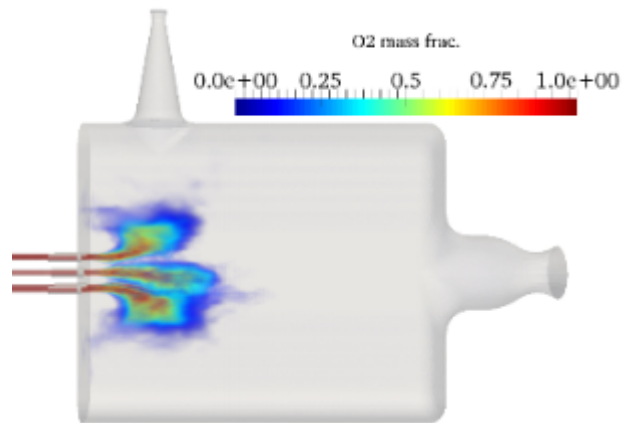
Fig. 6.   Meshed geometry.

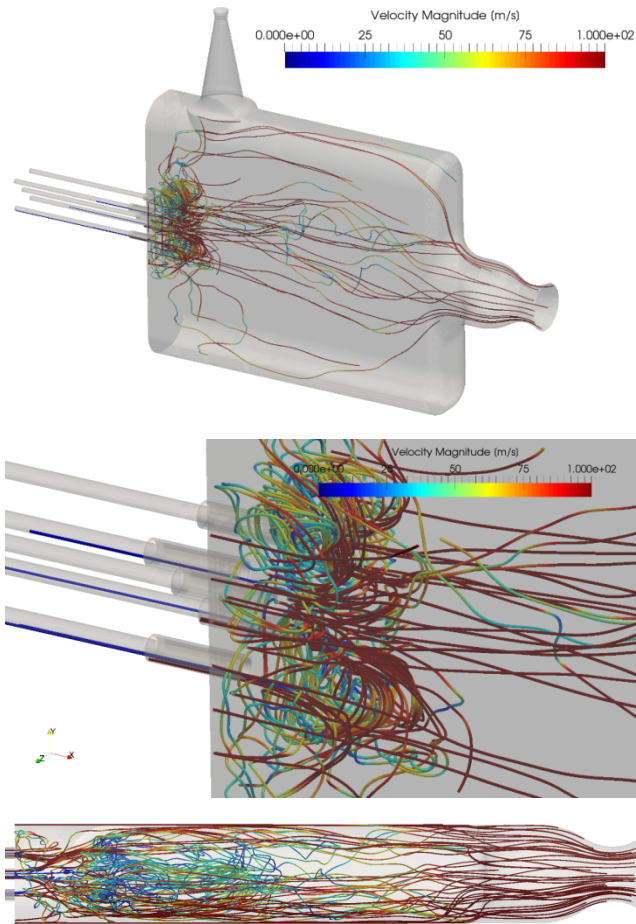Fig. 7.   Mean numerical O_2 mass fraction for unexcited case.

Fig. 8. Streamlines from the primary injectors for the unexcited case, viewed from the side (top), zoomed on the injectors (middle), and from above (bottom).

With the 2D view of the flow in the shadowgraph image in the upper half of Fig. 9, we are unable to infer the character of the flow field in the depth direction. Streamlines in the numerical result can be viewed from above, as in the bottom part of Fig. 8, providing flow field information from another point of view.

Looking in the near-injector region in Fig. 8, the streamlines indicate that there is relatively little recirculation from the primary injectors in the horizontal plane. The flames appear to be effectively confined by the window cooling flow. This is supported by examining the axial progression of propellant mass fraction distributions in the perpendicular plane in Fig. 10. The H_2 film cooling prevents the flames spreading to contact the window surfaces, causing them to spread vertically until they overlap by x = 50 mm.

4.2. Excited 1T-mode case

Coming now to the excited 1T-mode case, the impact of high amplitude, transverse acoustic velocity oscillations on the flames is considered.

The time-averaged impact of the 1T mode on the LOx cores as viewed from the side can be seen in the upper half of Fig. 11. Tracing of the core boundaries highlights how the cores are shortened and the outer cores are deflected vertically away from the chamber axis quite soon after injection. The agreement with numerical O_2 iso-surfaces in the lower half of

Fig. 11 is good.

As well as being shortened, the central core in Fig. 11 appears to taper to a point approximately 30 mm after injection. Examining the temporally resolved numerical results from other angles helps to explain this experimental observation. Atomisation of the LOx jet is driven by the passing acoustic waves. The velocity wave impinging from
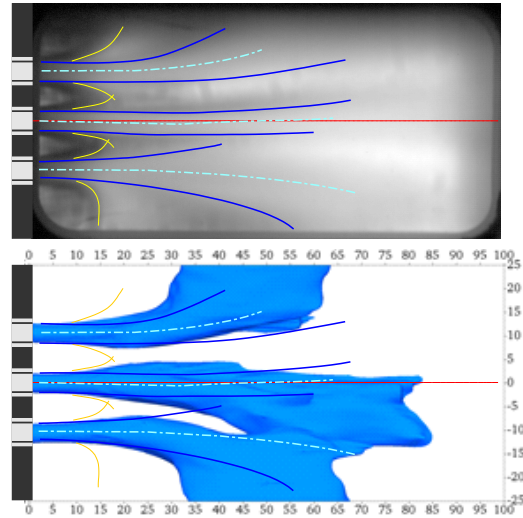

Fig. 9. Comparison of traced features from the time-averaged shadowgraph image (above) with numerical O_2 iso-surfaces of 10 kg/m^3 (below) for the unexcited case.
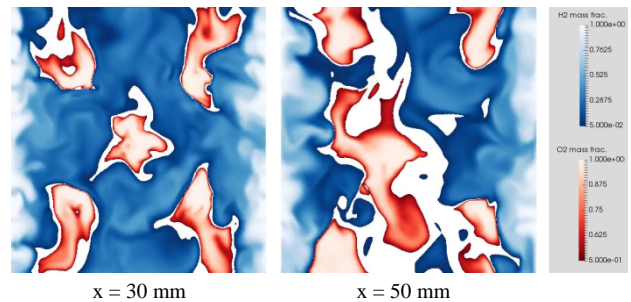

x = 30 mm　　　　　x = 50 mm

Fig. 10. Cross-sections of O_2 and H_2 mass fraction from the simulation at advancing axial locations for the unexcited case.
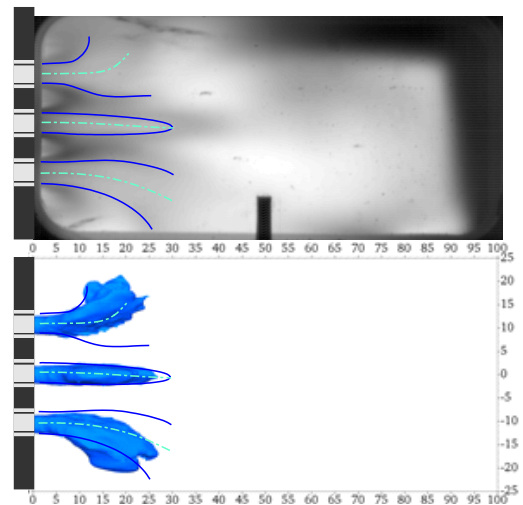

Fig. 11. Comparison of traced features from the time-averaged shadowgraph image (above) with numerical O_2 iso-surfaces of 10 kg/m^3 (below) for the excited 1T case.

above or below the jet causes it to flatten and spread in the direction perpendicular to the wave. This spreading can be seen in the O_2 iso-surfaces on the right side of Fig. 12, viewed from an off-angle, isometric perspective.

A further perspective on this effect is afforded by cross-sections of propellant mass fraction in Fig. 13. At the three positions advancing away from the injection plane, one sees the increasing flattening and lateral spreading of the LOx cores. The snapshots in Fig. 13 are taken from the same phase angle in the acoustic cycle, $\pi/2$, as the lower row in Fig. 12. This is when acoustic pressure is at its peak at the bottom of the combustion chamber, after the velocity wave has passed from top to bottom. The acoustic flow just passed has bent the sides of the flattened LOx core downwards. The sides of the core are less dense and become more easily entrained by the acoustic flow of surrounding gas. These 'wings' flap up and down, anchored at the dense centre of the core, when viewed in movies of the simulation results in Fig. 12 and Fig. 13.
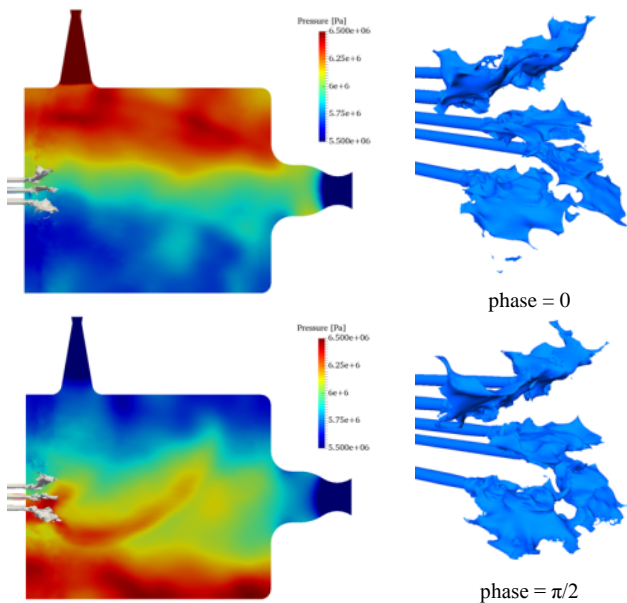

Fig. 12.   Snapshots from the simulation at phase angles of 0 (above) and $\pi/2$ (below) for the 1T-mode case, showing pressure (left) and O_2 iso-surfaces in the near-injector region.
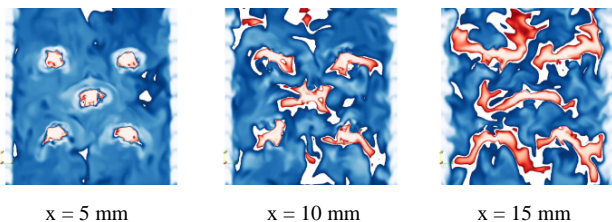

| x = 5 mm | x = 10 mm | x = 15 mm |

Fig. 13.   Cross-sections of O_2 and H_2 mass fraction from the simulation at advancing axial locations for the excited 1T-mode case.

This finding from the simulation explains well dynamics observed in the high-speed shadowgraph imaging. Lobes of increased intensity are seen alternately above and below the central LOx core during 1T-mode excitation. The lobes can be seen at phase angles of 0 and $\pi/2$ in phase-locked images in Fig. 14, extending from approximately 10 to 40 mm and broadening in the downstream direction. The form and

dynamics of the lobes is consistent with the movement of the low density O_2 'wings' of the flattened LOx core seen in the simulation.

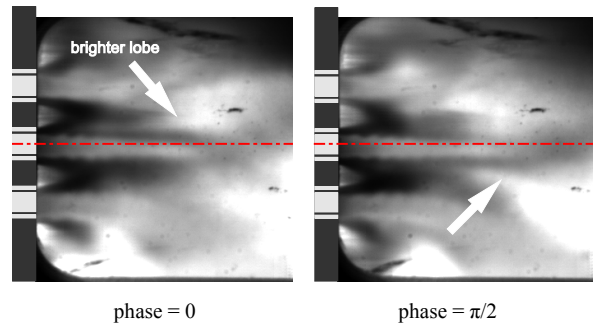

| phase = 0 | phase = $\pi/2$ |

Fig. 14.   Phase-locked shadowgraph images at phase angles of 0 (left) and $\pi/2$ (right) for the 1T-mode case.

5. Conclusion and outlook

The LES method was used to numerically model an experimental cryogenic rocket combustor with acoustic forcing. High-speed shadowgraph imaging of the multi-injector flow field is available to compare the acoustic response with the numerical simulation.

Whereas the experimental data is limited to imaging from a single point of view, the numerical simulation can provide information on the flow field throughout the combustion chamber volume. Accessing streamlines, species iso-surfaces, and species mass fraction distributions helped to explain the mechanisms of both steady and dynamic phenomena observed in the experimental data. Thus, the combination of experimental and numerical results improved the understanding of flame-acoustic interaction representative of thermo-acoustic combustion instabilities in cryogenic rocket engines.

A further aspect emphasised here is the improved interpretation of experimental observations based on the comparison with numerical simulation. Improved understanding of the experiment will allow the data to be better prepared for more focussed comparison between experimental and numerical results for the validation of modelling approaches. Optimised data preparation is currently underway for this purpose. Other test cases, for example excitation of the chamber longitudinal mode and other operating conditions, will also be addressed in future work.

References

1)   Preclik, D., and Spagna, P., "Low frequency and high frequency combustion oscillation phenomena inside a rocket combustion chamber fed by liquid or gaseous propellants," AGARD

Conference Proceedings, Neuilly Sur Seine, France: NATO Advisory Group for Aeronautical Research and Development, 1989.

2) Harrje, D. T., and Reardon, F. H., eds., Liquid propellant rocket combustion instability, Washington, DC: NASA SP-194, 1972.

3) Yang, V., and Anderson, W. E., eds., Liquid rocket engine combustion instability, Washington, DC: AIAA, 1995.

4) Hardi, J. S., Gomez Martinez, H. C., Oschwald, M., and Dally, B. B., "LOx jet atomization under transverse acoustic oscillations," Journal of Propulsion and Power, vol. 30, 2014, pp. 337–349.

5) Méry, Y., Hakim, L., Scouflaire, P., Vingert, L., Ducruix, S., and Candel, S., "Experimental Investigation of Cryogenic Flame Dynamics Under Transverse Acoustic Oscillations," Comptes Rendus Mécanique, vol. 341, Jan. 2013, pp. 100–109.

6) Rey, C., Ducruix, S., Richecoeur, F., Scouflaire, P., and Candel, S., "High Frequency Combustion Instabilities Associated with Collective Interactions in Liquid Propulsion," 40th AIAA/ASME/SAE/ASEE Joint Propulsion Conference & Exhibit, Fort Lauderdale, Florida: AIAA, 2004.

7) Richecoeur, F., Ducruix, S., Scouflaire, P., and Candel, S., "Experimental investigation of high-frequency combustion instabilities in liquid rocket engine," Acta Astronautica, vol. 62, Jan. 2008, pp. 18–27.

8) Sliphorst, M., Knapp, B., Gröning, S., and Oschwald, M., "Combustion Instability-Coupling Mechanisms Between Liquid Oxygen/Methane Spray Flames and Acoustics," Journal of Propulsion and Power, vol. 28, 2012, pp. 1339–1350.

9) Richecoeur, F., "Expérimentations et simulations numériques des interactions entre modes acoustiques transverses et flammes cryotechniques," École Centrale Paris, 2006.

10) Hardi, J., Beinke, S. K., Oschwald, M., and Dally, B. B., "Coupling of cryogenic oxygen-hydrogen flames to longitudinal and transverse acoustic instabilites," Journal of Propulsion and Power, vol. 30, 2014, pp. 991–1004.

11) Hardi, J. S., "Experimental investigation of high frequency combustion instability in cryogenic oxygen-hydrogen rocket engines," The University of Adelaide, Adelaide, Australia, 2012.

12) Hardi, J., Gröning, S., Webster, S. C. L., Beinke, S. K., Suslov, D. I., and Oschwald, M., "Review of experimental test cases for modeling high frequency combustion instability," 52nd AIAA/ASME/SAE/ASEE Joint Propulsion Conference & Exhibit, Cleveland, OH: AIAA, 2016.

13) Beinke, S. K., Banuti, D., Hardi, J. S., Oschwald, M., and Dally, B. B., "Modelling of a Coaxial LOx/GH2 Injection Element Under High Frequency Acoustic Disturbances," Progress in Propulsion Physics (in press), Torus Press, 2016.

14) Hashimoto, A., Murakami, K., Aoyama, T., Ishiko, K., Hishida, M., Sakashita, M., and Lahur, P., "Toward the Fastest Unstructured CFD Code 'FaSTAR'," 50th AIAA Aerospace Sciences Meeting including the New Horizons Forum and Aerospace Exposition, Nashville, Tennessee: AIAA, 2012.

15) Nicoud, F., and Ducros, F., "Subgrid-Scale Stress Modelling Based on the Square of the Velocity Gradient Tensor," Flow, Turbulence and Combustion, vol. 62, 1999, pp. 183–200.

16) Kitamura, K., and Shima, E., "Improvements of simple low-dissipation AUSM against shock instabilities in consideration of interfacial speed of sound," Proceedings of ECCOMAS CFD, 2010.

17) Chung, T. H., Ajlan, M., Lee, L. L., and Starling, K. E., "Generalized multiparameter correlation for nonpolar and polar fluid transport properties," Ind. Eng. Chem. Res, vol. 27, 1988, pp. 671–679.

18) Poling, B. E., Prausnitz, J. M., O'connell, J. P., and others, The properties of gases and liquids, Mcgraw-hill New York, 2001.

19) Ribert, G., Zong, N., Yang, V., Pons, L., Darabiha, N., and Candel, S., "Counterflow diffusion flames of general fluids: Oxygen/hydrogen mixtures," Combustion and Flame, vol. 154, 2008, pp. 319–330.

20) Li, J., Zhao, Z., Kazakov, A., and Dryer, F. L., "An updated comprehensive kinetic model of hydrogen combustion," International journal of chemical kinetics, vol. 36, 2004, pp. 566–575.

21) Bilger, R., "The structure of turbulent nonpremixed flames," Symposium (International) on Combustion, Elsevier, 1989, pp. 475–488.